International Journal of Coal Geology 196 (2018) 115–125

Contents lists available at ScienceDirect

International Journal of Coal Geology

journal homepage: www.elsevier.com/locate/coal

Potential permeability enhancement in Early Jurassic shales due to their swelling and shrinkage behavior

M.E. Houben[a,*], A. Barnhoorn[b], C.J. Peach[a], M.R. Drury[a]

[a] Faculty of Geosciences, Utrecht University, PO-box 80.021, 3508TA Utrecht, the Netherlands
[b] Faculty of Civil Engineering & Geosciences, Delft University of Technology, PO-box 5048, 2600GA Delft, the Netherlands

ABSTRACT

The presence of water in mudrocks has a largely negative impact on production of gas stored in these rocks, due to the fact that water causes swelling of the rock. Removing the water from the mudrock could potentially shrink the rock and increase the overall permeability of the rock. Investigation of the swelling/shrinkage behaviour of the rock during exposure to water vapour is of key importance in designing and optimizing unconventional production strategies. We have used outcrop samples of the Whitby Mudstone and the Posidonia shale, potential unconventional sources for gas in North-western Europe, to measure the swelling and shrinkage behaviour. Swelling and shrinkage of the rocks when exposed to water vapour was measured directly using 1 mm sample cubes in two different setups. The mm cubes were exposed to different levels of relative humidity either in an Environmental Scanning Electron Microscope (ESEM) or in a 3D dilatometer. Swelling of Whitby Mudstone and Posidonia shale is heterogeneous with 2–3 times more measured swelling strain perpendicular to the bedding. Volumetric swelling strains showed values between 0.6 and 2.2% for the Whitby mudstone and the Posidonia shale, respectively. The results suggest that it might be possible to increase permeability in the reservoir by decreasing the in-situ water activity due to shrinkage of the matrix.

1. Introduction

Due to their affinity for water clay minerals play an important role in the safety and economics of many industrial applications. For instance, shrinkage and swelling of clays determine the stability of soils and building foundations (e.g.: Abdullah et al., 1999; Das et al., 2010; Carrier et al., 2013; Erzin and Gunes, 2013), swelling of clays has important implications for drilling operations as it can cause wellbore instability (e.g.: Anderson et al., 2010). Contrastingly, clay swelling could be beneficial to seal off radioactive waste from the environment (e.g.: Delage et al., 2010). The impact of the swelling clays varies and depends on the mineralogy and the texture of the rock, hence the type of clay minerals present and their distribution within the rock (Abdullah et al., 1999; Aksu et al., 2015). The composition of the fluids present also plays a role, where the clay-water-electrolyte system is the main parameter affecting swelling (Abdullah et al., 1999; Aksu et al., 2015). During the drilling of oil and gas wells fluids are used. When water based drilling fluids are employed clay swelling can have a largely negative impact (e.g.: hole closure, casing problems, accumulation of drilled cuttings) on the drilling process significantly increasing well construction costs (Anderson et al., 2010). Due to the presence of swelling clays in the rock texture and/or due to the presence of mobilized clay particles in water-saturated rocks permeability of the reservoir is reduced (Aksu et al., 2015). The sorption induced swelling effects directly influence the opening and closure of pores and fractures in the rocks and influence the permeability, hence the productivity of reservoirs. Investigating the swelling/shrinkage behavior of the rock during exposure to water is of key importance in designing and optimizing unconventional production strategies. Removing the water from the mudrock could potentially shrink the rock and increase the matrix permeability (e.g. for coal: Fry et al., 2009; Liu et al., 2016a). Most studies of clay swelling have been focused on smectites due to their large swelling potential, where techniques have either investigated macroscopic properties such as the bulk volume change (de Jong et al., 2014) or the microscopic properties such as interlayer spacing (using for instance X-ray diffraction; Anderson et al., 2010; Carrier et al., 2013).

We are interested in the swelling and shrinkage of the naturally occurring mudstones the Posidonia shale and Whitby Mudstone (Houben et al., 2016a, 2016b). The Posidonia shale is a possible unconventional source for gas in the Netherlands (e.g.: Herber and de Jager, 2010; Van Bergen et al., 2013; Ter Heege et al., 2015) and the Whitby Mudstone is its time equivalent deposited in the UK in the same basin at the same time (e.g.: Powell, 2010). The Posidonia Shale and Whitby Mudstone are Toarcian age black shales occurring in the UK, France, the Netherlands, Germany and Luxemburg (e.g.: Littke et al., 1991; Hesselbo et al., 2000), and were deposited in an epicontinental sea at variable energetic conditions and periodic benthic oxygen

* Corresponding author.
E-mail address: m.e.houben@uu.nl (M.E. Houben).

https://doi.org/10.1016/j.coal.2018.07.003
Received 14 May 2018; Received in revised form 9 July 2018; Accepted 10 July 2018

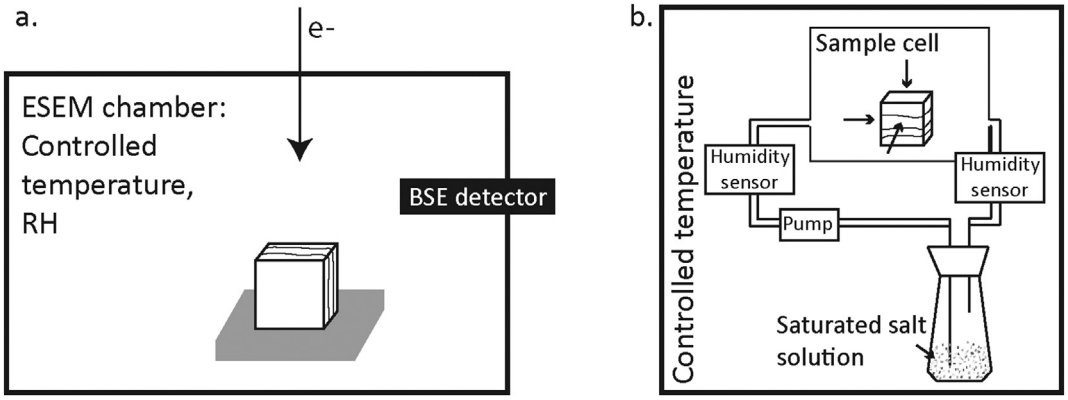

Fig. 1. a. Schematic drawing of a 1 mm cube sample in the ESEM chamber, where the area imaged was polished with a PIPS, and the area was imaged perpendicular to the bedding. b. Schematic drawing of the 3D dilatometer experimental set-up.

depletions (Trabucho-Alexandre et al., 2012; French et al., 2014). Mineral composition of the Posidonia Shale/Whitby Mudstone differs with location and height of the sample within the section (Houben et al., 2016a, 2016b). Organic matter content averges between 8 and 17%, Silicate content ranges between 15 and 25%, Carbonate content varies between 3 and 70% and sheetsilicate content varies between 25 and 85% (Chesapeake, 2010; Powell, 2010; Hilger, 2003; Klaver et al., 2012, 2016; Kanitpanyacharoen et al., 2012; Gasparik et al., 2014; Ghanizadeh et al., 2014; Rexer et al., 2014; Mathia et al., 2016; Houben et al., 2016a, 2016b; Douma et al., 2017). The carbonate and sheetsilicate content are highly variable per sample, whereas the silicate content is more constant and about 20% on average. The sheetsilicates seem to be mostly illite and interlayered illite/smectite, some kaolinite and minor amounts of chlorite (Houben et al., 2016b). The smectite is interlayered with illite in a ratio 80/20, meaning that smectite accounts for approximately 3% of the total mineralogy (Houben et al., 2016b) in the rocks. In the research presented here we have measured the amount of swelling and shrinkage of the Whitby Mudstone when exposed to different levels of relative humidity in 2D using an Environmental Scanning Electron Microscope (ESEM), in combination with measuring the volumetric change of a 1 mm cube of Whitby mudstone and Posidonia shale when exposed to different levels of relative humidity using a 3D dilatometer (Liu et al., 2016a).

2. Materials

2.1. Posidonia shale and Whitby mudstone samples

Samples used were Posidonia shale (Dotternhausen; PSFD) and Whitby Mudstone (Jet rock section; WMF) samples (Houben et al., 2016b). All investigated samples were outcrop samples collected during fieldwork (Posidonia shale - Dotternhausen, Germany; Whitby mudstone - Runswick Bay/Port Mulgrave, United Kingdom). Subsamples of 1 mm sized cubes were prepared in the Glass Workshop at Utrecht University, using a high precision digitally controlled diamond wafering saw, cooled by air. Many cubes were prepared simultaneously by first sawing a 1 mm thick wafer of clay which was afterwards sawed into cubes. The wafer was prepared parallel to the bedding meaning that the cubes were prepared from the same sample bed. The 1 mm cubes were dried at 50 °C in an oven prior to the experiments for at least 24 h, so that all samples investigated had a similar starting humidity.

3. Methods

3.1. ESEM

Ten 1 mm cubes were glued onto a Scanning Electron Microscope (SEM) stub using a carbon sticker so that the top sides of the cubes were oriented perpendicular to the bedding. The top side of all cubes were polished simultaneously using a Precision Ion Polishing System (PIPS; Fischione, SEM mill, model 1060). After polishing, a grid of 16 squares was deposited on some of the polished surface using the Pt target in the SEM (Nova Nanolab 600 FIB-SEM; De Winter et al., 2009; Liu et al., 2016b). The deposited squares were about 20 × 20 µm in size and spaced about 200 µm apart. Five polished cube surfaces were prepared with a grid, and five cube surfaces were polished while no grid was deposited on these surfaces. For all 10 polished top surfaces an SEM mosaic was made using a JEOL Neoscope II JCM-600 SEM. Based on the quality of the final polish three cubes were selected for investigation with an Environmental SEM (ESEM; Philips XL30 ESEM). All samples originated from the WMF4 sample block featuring a mineralogy of; 51.3% of sheetsilicates, 13.1% of silicates, 26.1% of carbonates, 0.8% of oxides, 7.7% of sulphides and 0.9% of sulfates (Houben et al., 2016a). The single sample cubes were exposed to different saturated vapour pressures at 0.5 °C inside the ESEM chamber so that the samples were exposed to a relative humidity varying between 0% and 100% depending on the pressure in the chamber (e.g.: Stokes, 2006). Fig. 1a shows for the experimental setup. By changing the vapour pressure in the ESEM chamber the relative humidity in the chamber changed. As soon as the pressure was stable the relative humidity in the chamber was stabilized as well. Pictures of the sample were always taken after the relative humidity in the ESEM chamber stabilized. Two of the sample cubes investigated (WMF4 Block 1 and WMF4 Block 2) had a Pt grid deposited on the top surface. Both sample cubes were firstly exposed to a relative humidity of 0% and after a calibration time of circa 1 h a picture of the whole polished surface was taken using a Back Scattered Electron (BSE) detector at a magnification of 100× (pixel size = 0.9 µm). Where after the pressure was increased enabling the relative humidity of the ESEM chamber to rise to 50%. After a calibration time of about 10 min exposing the sample to the new relative humid atmosphere the sample was imaged again with the BSE detector using a magnification of 100×. Next step was to increase the pressure in the ESEM chamber even more so that the relative humidity of the atmosphere in the ESEM chamber rose to 100%, and the sample was equilibrated for about 10 min in this atmosphere where after the sample was imaged again using the BSE detector at a magnification of 100×. After the relative humidity of the atmosphere had been increased to 100% it was decreased for WMF4 Block 1 to 0% and the samples was imaged again to compare the before and after dimensions of the sample. For WMF 4 Block 2 the relative humidity of the chamber was only increased from 0 to 100% and not decreased after. One other sample without Pt deposited grid (WMF Block 3) was used for swelling/shrinkage experiments, this samples was firstly exposed to a relative humidity of 0% in the ESEM chamber where after the relative humidity of the ESEM chamber was stepwise increased to 50% and to 100%. After the relative humidity had been up to 100% the humidity of the

ESEM chamber was decreased stepwise back to 50% and 0%.

The images taken at different relative humidities were used to digitally compare the dimensions of the samples, where both the Pt markers and the naturally occurring pyrite minerals were used as markers. Since both the Pt and the pyrite were white in the BSE images they could easily be segmented out of the image using thresholding in Matlab (Houben et al., 2013). The original images and the thresholded images where loaded into ArcGIS to convert the markers into polygons and to find the middle point of each of these polygons. The images covered a 2D surface perpendicular to the bedding meaning that the swelling and shrinkage parallel and perpendicular to the bedding could be measured in the same image.

3.2. 3D dilatometer

The swelling and shrinkage of the clay was measured directly using the 3D eddy-current dilatometer at Utrecht University (Liu et al., 2016a). The dimensions of a 1 mm cube were measured directly and continuously in three orthogonal directions inside the 3D dilatometer when the sample was exposed to different relative humid atmospheres. The 3D dilatometer uses three independent Lion Precision type ECL202 U3B eddy current sensors mounted in a stainless steel frame housing a sample stage at the center. The full scale of each eddy current sensor is 250 μm ± 12.5 nm at constant relative humidity (Liu et al., 2016a). We used 1 mm cubic samples that were fixed in position by the sample stage at three sides and could move freely in the other three directions. The experiments were performed on three 1 mm cubes, two samples of Whitby Mudstone (WMF4) and one sample of Posidonia Shale Dotternhausen (PSFD). The experimental set-up is shown in Fig. 1b, where the 3D dilatometer is situated inside a sealed glass chamber that is part of an air circulation circuit where the relative humidity is controlled by different solid salts in equilibrium with water vapour and aqueous salt solutions (Houben et al., 2014; Liu et al., 2016a). The whole set-up is enclosed in a temperature controlled box, where the temperature was set to 35 °C. For details on the working of the 3D dilatometer see Liu et al. (2016a). The samples were exposed to relative humidity values ranging from < 1% up to 95%, where the salts used were; Magnesium Chloride (32% RH), Magnesium Nitrate (50% RH), Sodium Chloride (75% RH), and Potassium Sulphate (95% RH). To get a low relative humidity phosphorus pentoxide powder (< 1% RH) has been used. For the stability of the relative humidity in the circuit, the stability of the temperature was controlled by a temperature controlled box around the circuit. A calibration of the relative humidity effect on the sensor signals can be found in appendix A in Liu et al. (2016a). The temperature of the sample and the three eddy current sensor signals were logged using a National Instruments logger at a sampling rate of 1 Hz. Relative humidity signals were also digitally logged using an independent system (EKH4views) at a sample rate of 0.1 Hz. Swelling displacement obtained from the eddy current sensors signals were measured as positive.

4. Results

4.1. ESEM

Sample Block 1 (WMF4) showed swelling and shrinkage when exposed to different humid atmospheres in the ESEM chamber (Table 1), main swelling and shrinkage happened perpendicular to the bedding. Block 1 showed a swelling strain of 0.3% perpendicular to the bedding and a swelling strain of −0.2% parallel to the bedding increasing the relative humidity in the ESEM chamber from 0 to 50%. Going from 0 to 100% relative humidity in the ESEM chamber resulted in a swelling strain of 1.4% perpendicular to the bedding and a swelling strain of 0.3% parallel to the bedding. Bringing the relative humidity within the ESEM chamber back to 0% after the 100% relative humidity was reached resulted in a swelling strain of −0.1% parallel to the bedding and 1.0% perpendicular to the bedding. Assuming that parallel to the bedding the sample shows an isotropic swelling strain the total volumetric swelling strain measured for this sample is 0.7%.

Sample WMF4 Block 2 showed more swelling than Block 1 when the relative humidity of the atmosphere in the ESEM was increased from 0 up to 100% (Table 1). For the whole sample we found an average of 1.4% swelling parallel to the bedding when the relative humidity in the ESEM chamber was increased from 0 to 50%, and a total of 1.6% swelling parallel to the bedding when increasing the relative humidity in the ESEM chamber from 0 to 100% (Fig. 2). Perpendicular to the bedding the average sample swelling was 2.2% increasing the relative humidity in the ESEM chamber from 0 to 50%, and 3.3% when relative humidity in the ESEM chamber was increased from 0 to 100%. Resulting in a volumetric swelling strain of 1.7% at a relative humidity increase from 0 to 50%. When the relative humidity in the ESEM chamber was increased from 0 to 100% the total volumetric swelling strain was 2.2%. Average strain varies throughout the sample and is measured only parallel and perpendicular to the bedding based on the markers deposited on the sample surface and the pyrite minerals naturally occurring in the samples microstructures. To illustrate the heterogeneity in the swelling and shrinkage a color code was used in Fig. 3. Bands that were swelling and shrinking more than average were indicated in red, yellow bands showed average swelling and shrinkage and green bands showed less than average swelling and shrinkage. These results show that parallel to the bedding the left half of the samples showed a higher amount of swelling strain than the right half of the samples. Perpendicular to the bedding the upper half of the sample showed less than average swelling strain when compared to the lower half of the sample. This demonstrates the heterogeneous swelling behavior of the sample and shows that in this orientation the sample block displayed most swelling in the lower left corner and least swelling in the upper right corner.

The last WMF4 sample investigated (Block 3) displayed perpendicular to the bedding 0.5% swelling strain when the relative was increased from 0 to 50%, and 0.8% swelling strain perpendicular to the bedding when the relative humidity was increased from 0 to 100% both measured on the sample overview (Table 1). Parallel to the bedding swelling strains measured were 0.3% (increasing the relative humidity from 0 up to 50% in the ESEM chamber) and 0.5% (increasing the relative humidity from 0 up to 100% in the ESEM chamber), when averaged over the whole sample. After the relative humidity in the ESEM was increased to 100% the relative humidity in the ESEM chamber was decreased stepwise back to 50% and to 0% relative humidity resulting in measured swelling strains of 0.6% and 0.4% parallel to the bedding and swelling strains of 1.3% and 0.9% perpendicular to the bedding. For sample WMF4 Block 3 images were not only taken at a magnification of 100×, imaging the whole 1 mm polished surface of the sample, but a magnification of 300× has also been used imaging a smaller area in the middle of the polished surface. Measured swelling strain was slightly higher when only considering the middle of the sample block (Table 1). Parallel to the bedding the measured swelling strains were 0.6 and 0.7% when the relative humidity in the ESEM was increased from 0% to 50% and from 0% to 100% respectively, perpendicular to the bedding this was 0.8% and 1.6% of swelling strain. Decreasing the relative humidity in the ESEM chamber back down to 50% the swelling strain parallel to the bedding was 0.8% and perpendicular to the bedding 1.3%. Reducing the humidity than caused shrinkages of the sample compared to the maximum volume at maximum relative humidity, but the volume was still increased when compared to the initial starting volume, hence there was still a positive swelling strain measured. Bringing the relative humidity down from 100% to 0% caused a swelling strain of 0.7% parallel to the bedding and 1.0% perpendicular to the bedding. The sample overview pictures (100× magnification) showed a volumetric swelling strain of 0.6%, whereas the 300× magnification pictures of the middle of the cube showed a volumetric swelling strain of 1% when was assumed that

Table 1
Swelling strain results for blocks 1 to 3 of sample WMF4 when exposed to different relative humid atmospheres in the ESEM.

RH (%)	Block 1 - overview			Block 2 -overview		
	// Bedding	⊥ Bedding	volumetric strain	// Bedding	⊥ Bedding	Volumetric strain
0	0.0	0.0	0.0	0.0	0.0	0.0
50	−0.2	0.3	0.0	1.4	2.2	1.7
100	0.3	1.4	0.7	1.6	3.3	2.2
50	–	–	–	–	–	–
0	−0.1	1.0	0.3	–	–	–
RH (%)	Block 3 - overview			Block 3 - 300× Magnification		
	// Bedding	⊥ Bedding	Volumetric strain	// Bedding	⊥ Bedding	Volumetric strain
0	0.0	0.0	0.0	0.0	0.0	0.0
50	0.3	0.5	0.4	0.6	0.8	0.7
100	0.5	0.8	0.6	0.7	1.6	1.0
50	0.6	1.3	0.8	0.8	1.3	1.0
0	0.4	0.9	0.5	0.7	1.0	0.8

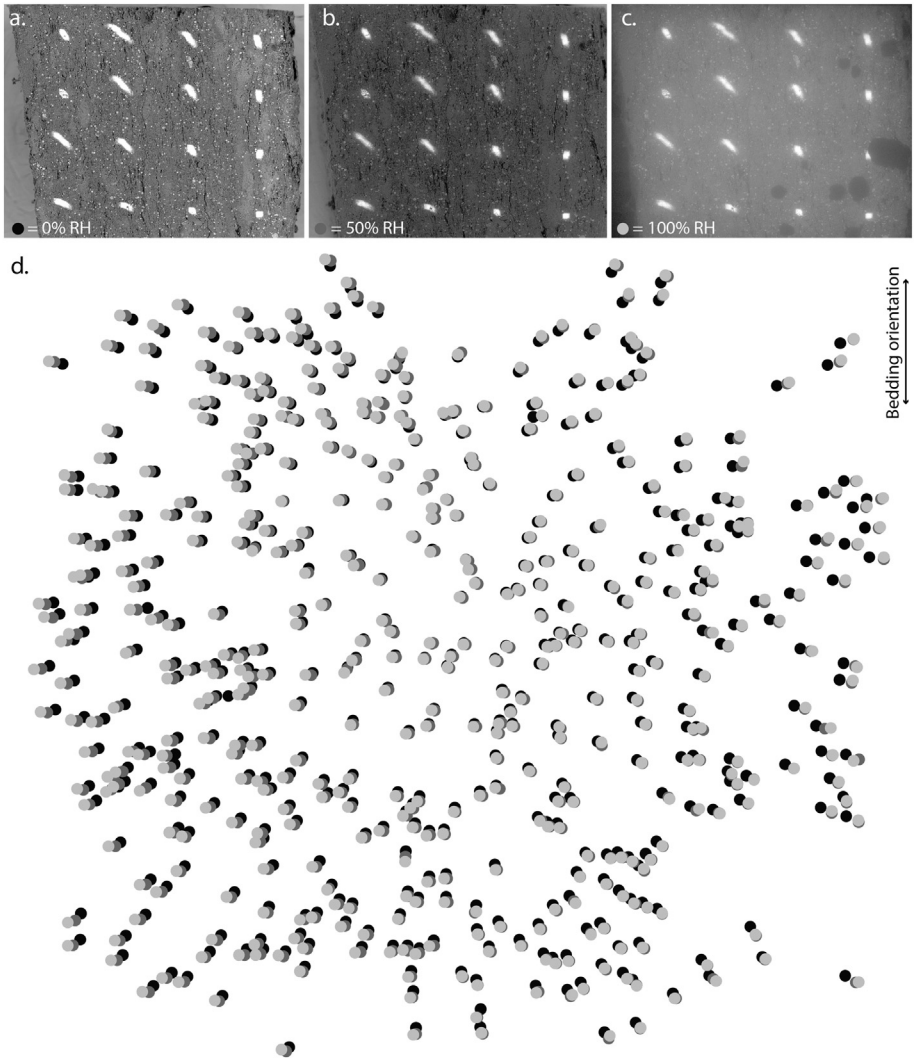

Fig. 2. a.-c. ESEM image of WMF4 Block 2 when exposed to different humid atmospheres in the ESEM chamber. d. The black circles (RH = 0%), dark grey circles (RH = 50%) and light grey circles (RH = 100%) show how the markers changed location during the experiment increasing the relative humidity in the ESEM chamber.

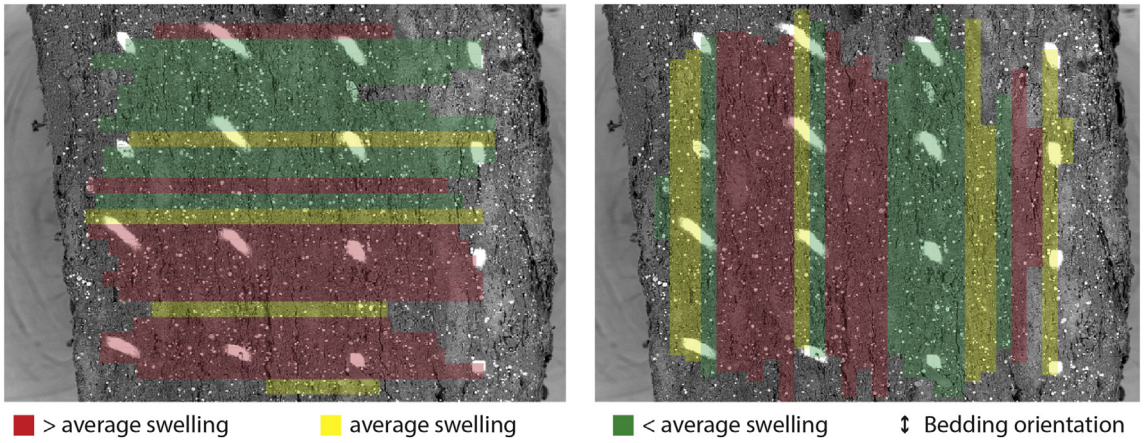

Fig. 3. Swelling strain as measured for samples Block 2 measured parallel and perpendicular to the bedding with respect to the average swelling strain.

Table 2
Corrected swelling strain in percent per sample per step. Relative humid atmosphere in the sample container was varied throughout the experiment and sample strain was measured in X, Y, and Z directions.

	PSFD - Cube A			PSFD - Cube B			PSFD - Cube C		
	Corrected swelling strain (%)			Corrected swelling strain (%)			Corrected swelling strain (%)		
RH (%)	x	y	z	x	y	z	x	y	z
0.5	0.00	0.00	0.00	0.00	0.00	0.00	0.00	0.00	0.00
22	0.03	0.06	0.13	0.04	0.02	0.11	–	–	–
33	0.06	0.11	0.19	0.03	−0.02	0.10	0.03	0.08	0.14
50	0.05	0.13	0.26	0.06	0.01	0.16	0.06	0.13	0.19
75	0.10	0.18	0.29	0.10	0.03	0.20	0.14	0.29	0.47
95	0.37	0.07	0.93	0.28	0.07	0.56	0.14	0.39	1.22
95	0.41	0.49	1.13	0.33	0.16	0.43	0.34	0.41	0.85
75	0.23	0.33	0.59	0.24	0.12	0.32	0.25	0.31	0.53
50	–	–	–	0.17	0.09	0.25	0.18	0.20	0.29
33	0.10	0.17	0.23	0.12	0.07	0.17	0.14	0.12	0.15
30	0.10	0.15	0.23	–	–	–	–	–	–
0.5	0.00	0.00	0.00	0.00	0.00	0.00	0.00	0.00	0.00
0.5	0.00	0.00	0.00	0.00	0.00	0.00	0.00	0.00	0.00
33	0.02	0.09	0.15	0.07	0.05	0.14	–	–	–
50	0.07	0.20	0.33	0.09	0.07	0.18	0.07	0.16	0.34
75	0.13	0.30	0.56	0.19	0.12	0.33	0.05	0.16	0.45
95	0.32	0.42	1.17	0.23	0.11	0.38	0.16	0.31	0.74
95	0.36	0.44	1.04	0.23	0.06	0.32	0.29	0.47	0.98
75	0.24	0.33	0.64	0.21	0.08	0.29	0.23	0.37	0.68
50	–	–	–	0.15	0.07	0.22	0.11	0.17	0.30
33	0.09	0.15	0.19	0.11	0.05	0.16	0.09	0.16	0.29
0.5	0.00	0.00	0.00	0.00	0.00	0.00	0.00	0.00	0.00

parallel to the bedding the swelling strain behaved comparable in both directions.

4.2. 3D dilatometer

We have used the 3D dilatometer at Utrecht University (Liu et al., 2016a) to measure the swelling and shrinkage of two 1 mm WMF4 cubes (A and C) and one 1 mm PSFD cube (B) in 3D. The Whitby Mudstone sample contains on average of 66% matrix (all grains with diameter smaller than 2 μm), 3% silicates, 20% carbonates, 4% of sulphates and 7% of organic matter (Houben et al., 2016b), where this mineralogy is based on SEM BSE images. The Posidonia shale (Dotternhausen) is mineralogically similar except that the organic matter content is higher and the matrix content is lower (56% matrix, 4% silicates, 22% carbonates, 2% sulphates and 16% organic matter; Houben et al., 2016b). The full set of results for all samples investigated here is presented in Table 2. Presented swelling strains were corrected in all directions (x, y and z) as specified by Liu et al. (2016a).

All samples show a roughly similar behavior when exposed to different levels of humidity. The swelling and shrinkage measured perpendicular to the bedding was larger (max. 1.1%) than parallel to the bedding (max. 0.4%) (Table 2, Fig. 4, Fig. 5), demonstrating heterogeneous swelling and shrinkage behavior with respect to the bedding. Also a slight difference can be observed between swelling and shrinkage in x and y directions (Fig. 4, Fig. 5), where sample WMF4-CubeA and WMF4-CubeC show slightly larger swelling and shrinkage in the y-direction and PSFD-CubeB displayed some more swelling and shrinkage in the x-direction. All the samples slowly expanded or shrank with time when relative humidity of the atmosphere around the samples was respectively increased or decreased (Fig. 5). Depending on the relative humidity of the atmosphere the samples changed their size and equilibrated in the current humid atmosphere in days up to weeks, where the humidity of the atmosphere changed within minutes. Some exceptions to this observation were visible. For example the first run with sample WMF4-cubeA where the y-direction sensor showed shrinkage when the relative humidity of the atmosphere was increased from 75% up to 95% whereas both sensors tracking swelling and shrinkage in the x and z directions showed swelling (Fig. 5). A second

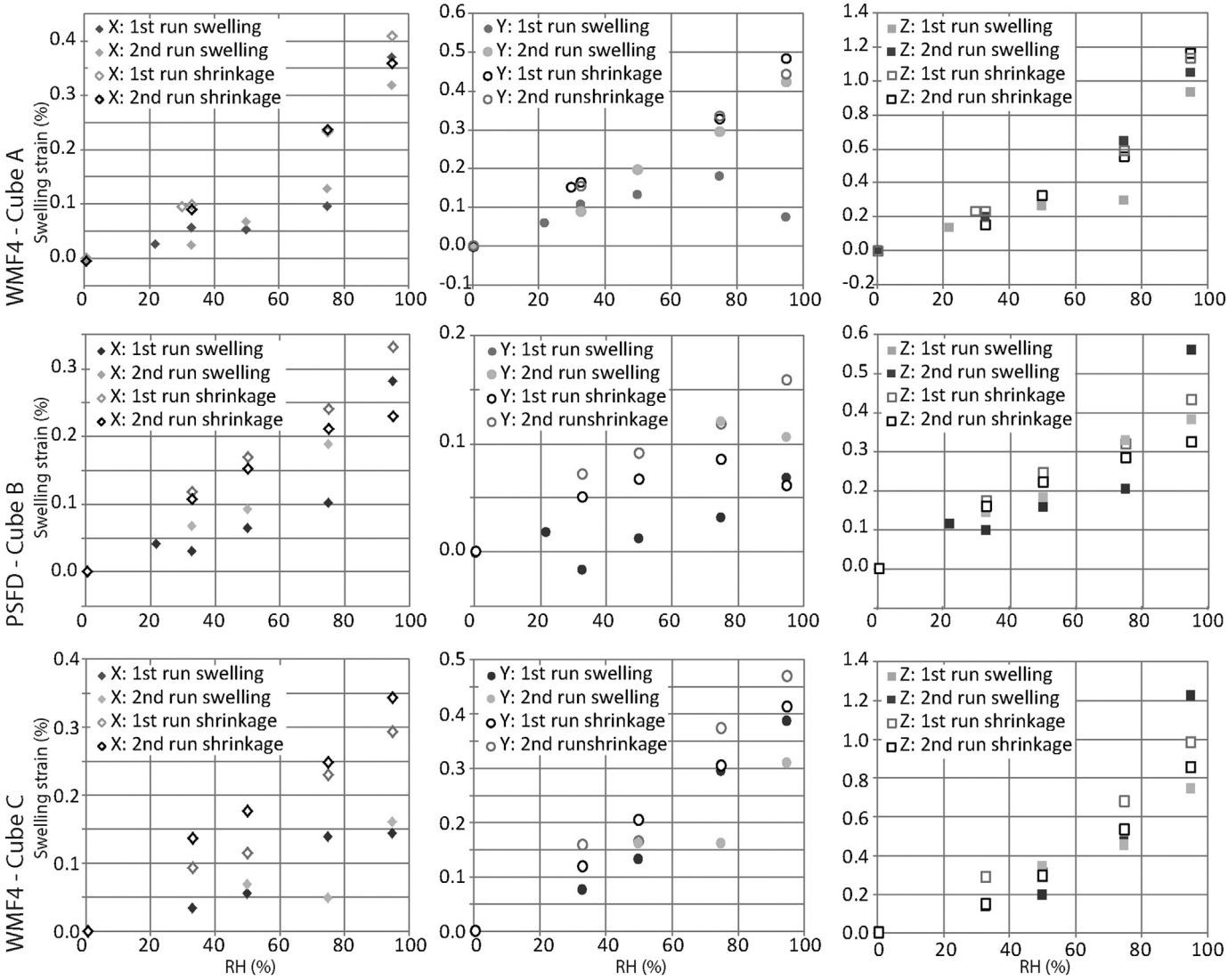

Fig. 4. Results of the swelling experiments in the 3D dilatometer showing swelling strain versus relative humidity in the sample container for 1st and 2nd run for all three samples.

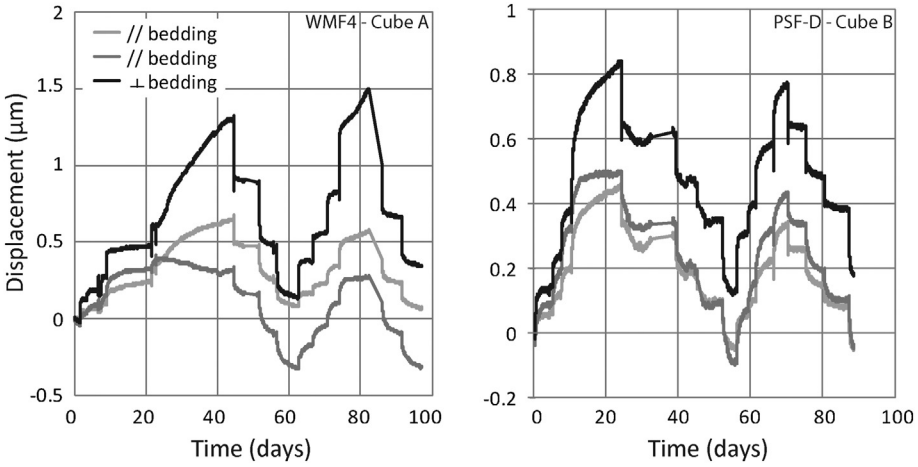

Fig. 5. Graph of the displacement in micrometer versus time in days for two samples (Cube A and Cube B). The experiments lasted for a little bit under 100 days in total and show two runs of increasing the relative humid atmosphere and decreasing it again.

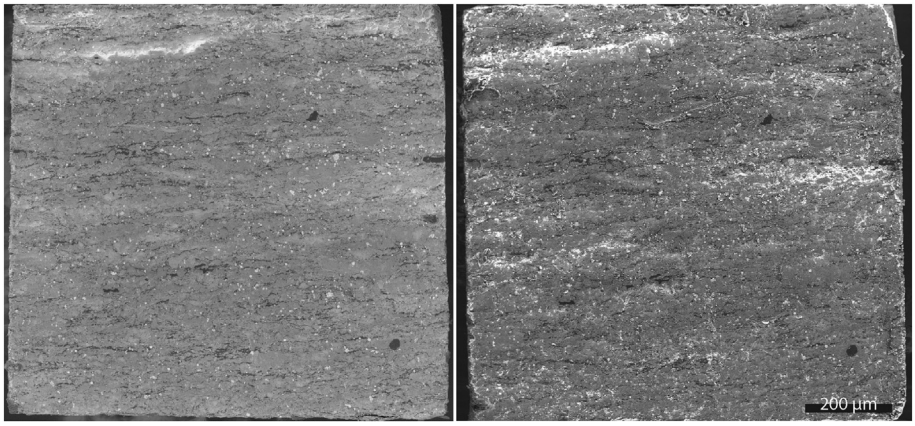

Fig. 6. Microstructural SEM images before and after the swelling experiment in the 3D dilatometer.

run with sample WMF4-cubeA of increasing and decreasing the relative humidity in the sample cell was performed and during that run when the relative humidity of the atmosphere was increased from 75% up to 95% all sensors showed swelling. For all samples the relative humidity in the atmosphere was increased from 0.5% up to 95% and back down to 0% twice resulting in not exactly the same but comparable results in total swelling and shrinkage per sample. Hysteresis was mostly observed in the experiments during the first cycle. Volumetric swelling strain was in the order of 1.8% in the case of WMF4-CubeA, 0.8% in the case of PSFD-CubeB and 1.0% in the case of WMF4-CubeC, so varied depending on the sample between 0.8 and 1.8%. Before and after pictures of one side of the 1 mm cube perpendicular to the bedding did not show obvious differences like the formation of new cracks visible in the picture taken after the experiments (Fig. 6) at the magnification used (200–270×).

5. Discussion

ESEM results are 2D and can be extrapolated to 3D when is assumed that perpendicular to the bedding the samples behave similar in both directions. That this is true for most cases on average is confirmed by the 3D dilatometer results showing similar swelling and shrinkage values perpendicular to the bedding in both x and y directions. During the ESEM experiments the time taken to equilibrate the sample within the humid atmosphere was a lot less than in the case of the 3D dilatometer experiments. The ESEM experiments took a couple of hours in total, whereas using the 3D dilatometer the experiments lasted for 1–3 months. This was due to the fact that for the 3D dilatometer experiments we had the opportunity to wait until the sample was in equilibrium with the humid atmosphere (up to 2 weeks) and we changed the humidity of the atmosphere only after the samples did not show swelling/shrinkage anymore (Fig. 5), whereas during the ESEM experiments we let the sample equilibrate with the current atmosphere for 10–60 min inside the ESEM chamber where after the pictures were taken and the humidity of the atmosphere in the ESEM chamber was changed. The 3D dilatometer results show that most of the irreversible deformation took place during the first cycle of increasing and decreasing the atmospheres humidity, whereas the 2nd cycle showed mostly reversible swelling and shrinkage. The ESEM results showed less reversible swelling and shrinkage, which we assumed is mainly due to the fact that we exposed the sample a shorter amount of time to the different levels of relative humidity, which is especially visible when decreasing the humidity in the ESEM after it reached its maximum. The ESEM samples do not shrink back entirely and do not fully recover to the sample size with which they started out. This leads to the conclusion that initial swelling is faster than initial shrinkage. The heterogeneity in swelling within the 1 mm cube investigated using the ESEM (Fig. 3) is most likely due to microstructural differences in the different layers. Certain layers having a mineralogy/porosity that swell/shrink easier than others. Since the representative elementary area (REA) for microstructures is 150 by 150 µm (Houben et al., 2016a), the overall swelling should not be measured on area's smaller than that. Fig. 3 shows that swelling is a heterogeneous process on the sub-mm scale and that there are areas that react faster to a humidity change in the atmosphere than others.

Average volumetric swelling strains measured using the ESEM method when the relative humidity of the atmosphere was increased from 0% to 100% ranged between 0.7% and 2.2%, whereas volumetric swelling strains using the 3D dilatometer method when increasing the relative humidity of the atmosphere from 0.5% to 95% ranged between 0.4% and 0.7% for the WMF and between the 0.2% and 0.3% for the PSFD. Hence the swelling/shrinkage results of the 3D dilatometer are slightly lower than the ESEM results for the WMF, which could be due to; the different equilibration times, the difference in the relative humidity being slightly lower at maximum for the 3D dilatometer experiments, or naturally occurring mineralogical differences within the samples. In addition, the 3D dilatometer results were corrected for the effect of the relative humidity whereas for the ESEM results the data was not corrected for a potential effect of imaging at different humidity values in the atmosphere of the ESEM. The PSFD shows less swelling and shrinkage overall than the WMF samples when measurements were performed using the 3D dilatometer, which could be due to microstructural differences. Porosity is slightly lower for the PSFD samples as well as that the clay matrix content is lower and the organic matter content is higher for the PSFD (Houben et al., 2016a, 2016b). Both methods showed that swelling strain is anisotropic and that 2–3 times more swelling strain was measured perpendicular to the bedding than parallel to the bedding on average (Fig. 7). The swelling anisotropy ratio is the equilibrium swelling strain in Z-direction compared to the average equilibrium swelling strains in X and Y directions (Liu et al., 2016a). During the 1st experimental cycle (upward pointing triangles in Fig. 7) it looks like slightly more swelling anisotropy was measured than when the relative humidity was decreased (downwards pointing triangles in Fig. 7), this is due to the fact that the 1st cycle of the experiment was less reversible than the 2nd cycle. The ESEM method shows that not only there is a difference in swelling strain measured parallel and perpendicular to the bedding. Swelling strain also varies when measured in the same direction depending on location within the sample (Fig. 3). The differential swelling within the samples can cause extra stress build-up and closure of pores and cracks in parts of the sample when the sample is under confined conditions, but also extra pore and crack opening in the areas that experience less swelling.

The swelling anisotropy ratio is on average slightly larger than the one found for coal (Liu et al., 2016a), indicating more anisotropic behavior for the investigated shales. The anisotropic swelling behavior of the Whitby mudstone is proposed to be due to the sheetsilicates, pores

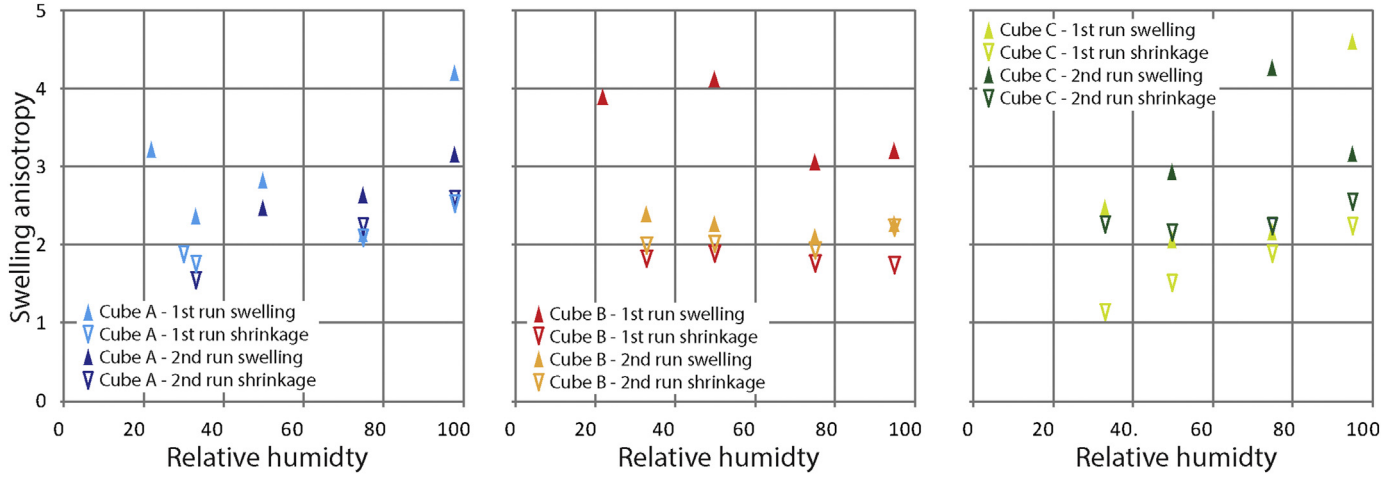

Fig. 7. Swelling anisotropy ration versus relative humidity plotted for all samples. Upward facing triangles mean that the points refer to measurements when the relative humidity in the cell was increased, whereas the downward facing triangles where measured during relative humidity decrease.

and cracks present oriented parallel to the layering/ bedding plane in the rocks (e.g.: Zhang et al., 2010). Zhubayev et al. (2015) showed that the attenuation anisotropy in the Whitby Mudstone could be as large as 70% for dried samples and that the closure/opening of microcracks is a dominant mechanism changing the attenuation anisotropy. Attenuation anisotropy was generally largest perpendicular to the bedding (Zhubayev et al., 2015). Things like anisotropic distribution of microfractures, non-linear elastic swelling behavior of the sheetsilicates, anisotropic water vapour access in the matrix, pore network and pore orientation, preferred orientation of adsorption sites, multiple layer adsorption, all play a role (see also Liu et al., 2016a for coal). For instance, more microfractures in an area could mean that the particular area is easier accessible for water, hence could swell/shrink more easily, and the same goes for a better developed pore network in a certain area. When more clay minerals are present in an area that is easy accessible for water cause swelling/shrinkage anisotropy, as well as the tendency of clay minerals to swell/shrink more in a certain direction.

Ewy (2015) showed that shales easily change their water contents when exposed to air with a lower or higher than the current relative humidity. Loss of water could be damaging to the shales due to the development of drying cracks (e.g.: Soe et al., 2009; Houben et al., 2014; Ewy, 2015). The 1 mm cubes used in the experiments show drying cracks prior to the swelling and shrinkage experiments, but do not reveal visual change in terms of damage due to the swelling and shrinkage cycling when investigated with an SEM (JEOL Neoscope II JCM-600) at low resolution (200–270×) before and after the experiment (Fig. 6). The cubes investigated using the ESEM method do show an increase in width of certain cracks with an increase in relative humidity, Fig. 8 shows an increase of one pixel (0.9 μm) in crack width when relative humidity went up from 0 to 100%. Ewy (2015) showed that the average swelling strain decreases with increasing effective confining stress for all samples and fluids investigated. Since the experiments described in this paper were performed under unconfined conditions and the fluid used was water vapour the average swelling of the investigated samples can be compared to the DI H2O data of Ewy (2015) showing an average swelling strain of ca. 1.2% for sample ShaleG which has a higher porosity but a similar mineralogy as the early Jurassic shales investigated here. Zhang et al. (2010) found higher volumetric swelling strains of about 8–10% for the Opalinus clay and the Callovio Oxfordian clay after wetting of unconstrained samples for 2 months at 23% RH and 8 months at 100% RH. Minardi et al. (2016) found more similar swelling strain results to ours and the results of Ewy (2015) for the Shaly facies of Opalinus clay. Minardi et al. (2016) show one wetting and one drying curve for an Opalinus clay sample and the corresponding changing volumetric swelling strain when changing the relative humidity of the atmosphere from 50% up to about 95% and back down to about 40%. The swelling strain for the Shaly facies of Opalinus Clay is in the order of 1.5% and the swelling strain perpendicular to the bedding is about three times as large as the swelling strain parallel to the bedding (Minardi et al., 2016). This is comparable to the Whitby Mudstone and Posidonia Shale (Dotternhausen) results for which the swelling strain parallel to the bedding is 2–3 times less than

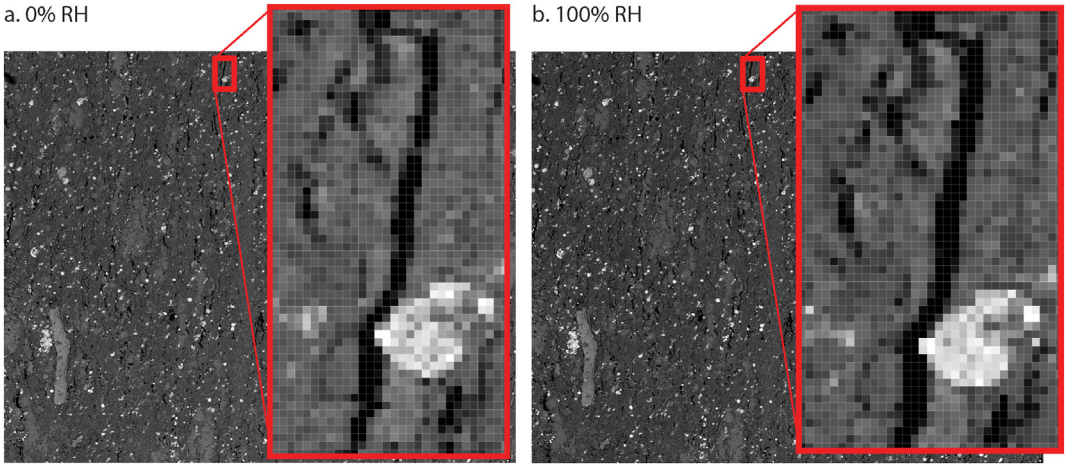

Fig. 8. ESEM pictures taken at different relative room humidity illustrating the increase in crack width when increasing relative humidity.

the swelling strain perpendicular to the bedding. In addition, Zhang et al. (2010) state that a higher clay content resulted in more shrinkage, which was confirmed by the data published in this paper. Furthermore, Ewy (2014) observed that the higher the compaction of the clay the less amount of swelling strain it displays. This implies that the fact that the Posidonia shale (Dotternhausen) shows less swelling strain than the Whitby Mudstone could be due to mineralogical differences, but a difference in compaction rate should also be considered, or a combination of both. Compaction rates depend on local stress state, but also on initial porosity and amount of clay minerals present (Dewhurst and Aplin, 1998; Broichasen et al., 2005), next to the presences and distribution of large resistant minerals (Houben et al., 2014).

6. Theory versus experiments: relationship between equilibrium swelling strain and RH

Volumetric swelling strain measured for the Whitby Mudstone is about half of the swelling strain measured for coal by Liu et al. (2016a). Liu et al. (2016a) came up with a number of models to compare the volumetric swelling strains versus activity of water vapour. One could use these models to see whether they can explain our results for claystones as well, the models are:

1. The HS model (Hol and Spiers, 2012; Liu et al., 2016a): $e_v^{eq} = \frac{C_s K a_g}{1 + K a_g} \rho V_0$, where e_v^{eq} is the equilibrium volumetric swelling strain, C_s is the total number of localized adsorption sites available for water present in one kilogram of rock, K is the equilibrium constant for adsorption, a_g is the water vapour activity, ρ is the density of the rock and V_0 is the bulk volume change of the matrix due to adsorption of one mole of water molecules;
2. The Dent-based case (Liu et al., 2016a): $e_v^{eq} = \left(\frac{K_1 a_g}{1 - K_2 a_g + K_1 a_g} + \frac{K_1 K_2 a_g^2}{(1 - K_2 a_g)(1 - K_2 a_g + K_1 a_g)}\right) \rho V_0 C_s$, where K_1 and K_2 are the equilibrium constants for primary and secondary adsorption respectively;
3. The DW based case (Liu et al., 2016a): $e_v^{eq} = \left(\frac{C_{s1} K_1 a_g}{1 + K_1 a_g} + \frac{C_{s2} K_2 a_g}{(1 - K_2 a_g)}\right) \rho V_0$, where C_{s1} and C_{s2} are the concentrations of water molecules associated with primary and secondary adsorption respectively.

Measuring values like the number of localized adsorption sites, the equilibrium constant for adsorption and the bulk volume change of the matrix due to adsorption of one mole of water was beyond the scope of this paper. Assuming that the organic matter is rate controlling by swelling though validates the use of the same values as used for coal for the number of localized adsorption sites, the equilibrium constant for adsorption, and the bulk volume change of the matrix due to adsorption of one mole of water. Using the 'coal' values though generates higher modeled values for the equilibrium volumetric swelling strain than the ones measured experimentally. Assuming a mudstone rock density of 2400 kg/m^3 (Douma et al., 2017) the models (Liu et al., 2016a; Hol and Spiers, 2012) predict a volumetric swelling strain of 1.8–1.9%. Only about 6–9% of the matrix of WMF4 (Houben et al., 2016b) is made out of organic matter, meaning that about 0.1% of swelling strain can be caused by swelling of the organic matter. The measured volumetric swelling strain for sample WMF4 is in the range of 0.2–0.7% (Fig. 9), meaning that the organic matter swelling can account for some of the volumetric swelling strain we have measured, but the clay minerals contribute to the total volumetric swelling of the sample as well. Most likely would be that not only the equilibrium constant for adsorption is different in claystones, but also the total number of localized adsorption sites is different. Seemann et al. (2017) investigated the water vapour sorption on a number of different claystones. They have measured the monolayer capacity for water on different claystones to be between 0.11 and 0.73 mol/kg. This range of monolayer sorption values can be used in the models (Liu et al., 2016a; Hol and Spiers, 2012) to exchange the number of localized adsorption sites for water present in one kilogram of coal (C_s) to the values for claystones. Keeping all the other values similar to the coal values than generates two end-member results for the three different models. The HS model shows volumetric swelling strains between 0.02 and 0.1% which are lower than the ones measured in the experiments (Fig. 9b), the Dent-based model yields values between 0.2 and 1.2%, and the DW-based model shows values between 0.3 and 1.8%. Again experimental data is best explained by the Dent-based and DW-based models and with a C_s value that are similar the lower end values of the ones measured by Seemann et al. (2017). Instead of using the Seemann et al. (2017) values one could also use the values for volume swelling per gram of dry shale as measured by Ewy (2014) on different shales to substitute the values for C_s times V_0 in the models. Ewy (2014) reported values between 0.000001 and 0.00006 m^3/kg, with most of the clays showing values between 0.000001 and 0.000015 m^3/kg. Keeping the constant for the clay matrix adsorption the same as for coal generates two end member results that envelope the data in the case of the HS model. The Dent-based and the DW-based models fit the experimental data best when the lowest values for C_s times V_0 were used (Fig. 9c). Best fits for all models are presented in Fig. 9d. One can predict the amount of swelling of the shales until a certain extent, where the DW-based and Dent-based models can better explain the experimental data than the HS model. This indicates that the swelling of clay is not well explained when it is assumed that the swelling solely depends on the adsorption of the first layer of water molecules or solely depends on monolayer adsorption with strong binding energy (Liu et al., 2016a).

7. Implications

The results show swelling of the Whitby Mudstone and Posidonia Shale when the sample is exposed to a more humid atmosphere than before and shrinkage of the sample when the relative humidity of the atmosphere is decreased. This result suggests that one will be creating space (about 1–2%) by drying due to shrinkage of the shales. We did not see the formation of cracks during the swelling and shrinkage experiments at the scale used for investigation, we did see that earlier formed cracks were becoming wider when the relative humidity of the atmosphere increased (at unconfined conditions). Assuming that the Youngs modulus of these samples is comparable to what Douma et al. (2017) measured for the Whitby Mudstone (10–15 GPa), the stress needed to get 1–2% of strain is in the order of 100–300 MPa, these values are quite high when you compare it to experimental values. Uniaxial compression experiments show that you need 40–50 MPa axial stress to generate 1% strain and 50–70 MPa axial stress to generate 2% strain (Barnhoorn et al., 2018), indicating that 1–2% of strain will generate cracks, hence will improve the permeability of the rock depending on the local stress state. Additionally, one has to keep in mind that when the material shrinks you are decreasing the permeability of the undamaged matrix due to the fact that pores will become smaller and pore pathways might close off due to the fact that pore throats can close. Creating cracks spaced relatively close together due to shrinkage of the rock though would increase the permeability of the overall rock more than the permeability will be reduced by matrix shrinkage. Main controls will be the crack width of the open cracks, whether or not there is a fluid present in the cracks, and whether or not an open fracture network is created that connects fractures together or that connects fractures to the existing percolating pore network. By how much the permeability of the rocks improves will depend on the rock and the geological setting the rock is in. Even though pretty similar in composition, Posidonia shale and Whitby Mudstone, already showed different amounts of volumetric swelling strains, where the two Whitby Mudstone samples yielded comparable results. In situ the clays could show more swelling and shrinkage effects, since the samples before the experiments were already dried and could have suffered from some permanent changes to the microstructure before the experiments started.

Although the smectite component in the clays investigated here is

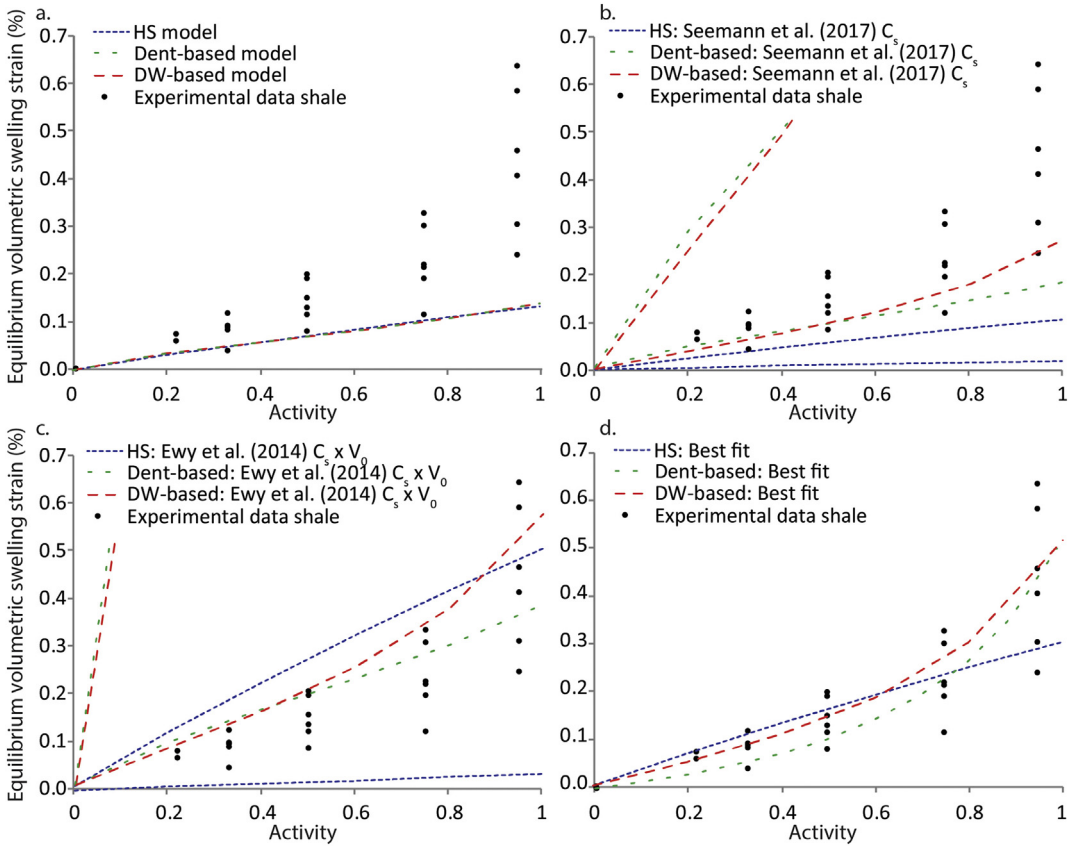

Fig. 9. Volumetric swelling strain at equilibrium versus water vapour activity, using methods as described by Liu et al. (2016a). Adopting the models by Liu et al. (2016b). The models (Hol and Spiers, 2012; Liu et al., 2016) with the number of localized adsorption sites for water present in one kilogram of coal (C_s) exchanged to the values for claystones as reported by Seemann et al. (2017). c. The models (Hol and Spiers, 2012; Liu et al., 2016a, 2016b) with volume swelling per gram of dry shale as measured by Ewy (2014). d. Best fits of the models to the experimental data.

low (circa 3%), the samples still show considerable amounts of swelling, where the main swelling/shrinkage component seems to be the clay matrix (all minerals with diameters < 2 μm, where the clay minerals present are mainly illiet, interlayered illit/smectite and kaolinite (Houben et al., 2016a)) since the PSFD sample with lower contents of clay minerals showed less swelling. Hence, although small, there is a potential for desorption-induced matrix shrinkage and crack opening to enhance permeability. In this case, the matrix shrinkage could be enhanced by exposure to liquid nitrogen at cryogenic temperatures since samples that are freeze-dried lose more water than samples exposed only to vacuum or elevated temperatures up to 105 °C (Houben et al., 2013; Desbois et al., 2014; Liu et al., 2016a).

8. Conclusions

We have investigated the swelling and shrinkage behaviour of the Whitby mudstone and Posidonia shale. Although the gas shales comprise little swelling clays (< 3% of smectite), the swelling and shrinkage of the rocks was measurable when the rocks were exposed to different relative humidity. The relative volumetric change was in the order of 0.4–2.2 vol% for the Whitby mudstone. The swelling and shrinkage depended on the measuring direction with respect to the bedding, where maximum swelling/shrinkage occurred perpendicular to the bedding. Anisotropy in swelling/shrinkage orientation is due to preferred alignment of the sheetsilicates, which were found to be the main cause found for swelling/shrinkage. Parallel to the bedding the swelling/shrinkage measured was less, but a similar values was measured in both directions parallel to the bedding. ESEM results showed that swelling was microstructure dependent with areas that showed more swelling and shrinkage and areas that were less affected. The swelling/shrinkage potential of the rock is mostly dependent on the amount of clay minerals present in the rock, since the rock with less clay minerals and more organic matter (PSFD) showed less volumetric swelling. Exposing the rocks to less and more relative humidity caused the matrix to expand and shrink, hence caused micro-crack opening and closing with potential permeability enhancement. The swelling/shrinkage of the rocks can be modeled where the more general case that swelling is caused by both primary and secondary adsorption does explain the experimental data best.

Acknowledgements

Eimert de Graaff is thanked for helping out with the 3D dilatometer set-up at Utrecht University, and Jinfeng (Ross) Liu is thanked for explaining how to use that set-up. Arjan Thijssen is thanked for operating the ESEM system at TUDelft. Funding by the Topsector Energy Innovation Program upstream gas (TKIG01017), our industry partners (EBN, Engie, Wintershall) through the 2f2s program, and NWO (016.Veni.171.041) is greatly appreciated. Two anonymous reviewers are thanked for their constructive reviews that helped improve the manuscript.

References

Abdullah, W.S., Alshibli, K.A., Al-Zou'bi, M.S., 1999. Influence of pore water chemistry on the swelling behavior of compacted clays. Appl. Clay Sci. 15, 447–462.
Aksu, I., Bazilevskaya, E., Karpyn, Z.T., 2015. Swelling of clay minerals in unconsolidated porous media and its impact on permeability. GeoResJ 7, 1–13.
Anderson, R.L., Ratcliffe, I., Greenwell, H.C., Williams, P.A., Cliffe, S., Coveney, P.V., 2010. Clay swelling – a challenge in the oilfield. Earth Sci. Rev. 98, 201–2016.
Barnhoorn, A., Verheij, J., Frehner, M., Zhubayev, A., Houben, M., 2018. Experimental

identification of the transition from elasticity to inelasticity from ultrasonic attenuation analyses. Geophysics 83 (4), MR221–MR229.
Van Bergen, F., Zijp, M., Nelskamp, S., Kombrink, H., 2013. Shale Gas Evaluation of the Early Jurassic Posidonia Shale Formation and the Carboniferous Epen Formation in the Netherlands. In: Chateliers, J., Jarvie, D. (Eds.), Critical Assessment of Shale Resource Plays. Vol. 103. AAPG Memoir, pp. 1–24.
Broichasen, H., Littke, R., Hantschel, R., 2005. Mudstone compaction and its influence on overpressure generation, elucidated by a 3D case study in the North Sea. International Journal of Earth Science 94, 956–978.
Carrier, B., Wang, L., Vandamme, M., Pellenq, R.J.-M., Bornert, M., Tanguy, A., Van Damme, H., 2013. ESEM study of the humidity-induced swelling of clay film. Langmuir 29, 12823–12833.
Chesapeake, 2010. Posidonia Cutting Research, 26th of July 2010. www.nlog.nl available through.
Das, S.K., Samui, P., Sabat, A.K., Sitharam, T.G., 2010. Prediction of swelling pressure of soil during artificial intelligence techniques. Envrion. Earth Sci. 61, 393–403.
de Jong, S.M., Spiers, C.J., Busch, A., 2014. Development of swelling strain in smectite clays through exposure to carbon dioxide. Int. J. Greenh. Gas Control 24, 149–161.
Delage, P., Cui, Y.J., Tang, A.M., 2010. Clays in radioactive waste disposal. J. Rock Mech. Geotech. Eng. 2, 111–123.
De Winter, D.A.M., Schneijdenberg, C.T.W.M., Lebbink, M.N., Lich, B., Verkleij, A.J., Drury, M.J., Humber, B.M., 2009. Tomography of insulating biological and geological materials using focused ion beam (FIB) sectioning and low-kV BSE imaging. J. Microsc. 223 (3), 372–383.
Desbois, G., Urai, J.L., Hemes, S., Brassinnes, S., de Craen, M., Sillen, X., 2014. Nanometer-scale pore fluid distribution and drying damage in preserved clay cores from Belgian clay formations inferred by BIB-cryo-SEM. Eng. Geol. 179, 117–131.
Dewhurst, D.N., Aplin, A.C., 1998. Compaction-driven evolution of porosity and permeability in natural mudstones: an experimental study. J. Geophys. Res. 103 (B1), 651–661.
Douma, L.A.N.R., Primarini, M.I.W., Houben, M.E., Barnhoorn, A., 2017. The validity of generic trends on multiple scales in rock-physical and rock-mechanical properties of the Whitby mudstone, United Kingdom. Mar. Pet. Geol. 84, 135–147.
Ewy, R., 2014. Shale swelling/shrinkage and water content change due to imposed suction and due to direct brine contact. Acta Geotech. 9, 869–886.
Ewy, R., 2015. Shale/claystone response to air and liquid exposure, and implications for handling, sampling and testing. International Journal of Rock mechanics & Mining Sciences 80, 388–401.
French, K.L., Sepúlveda, J., Trabucho-Alexandre, João, Grocke, D.R., Summons, R.E., 2014. Organic geochemistry of the early Toarcian oceanic anoxic event in Hawsker bottoms, Yorkshire, England. Earth Planet. Sci. Lett. 390, 116–127.
Fry, R., Day, S., Sakurovs, R., 2009. International Journal of Coal Preparation and Utilization 29, 298–316.
Gasparik, M., Bertier, P., Gensterblum, Y., Ghanizadeh, A., Krooss, B.M., Littke, R., 2014. Geological controls on the methane storage capacity in organic-rich shales. Int. J. Coal Geol. 123, 34–51.
Ghanizadeh, A., Gasparik, M., Amann-Hildenbrand, A., Gensterblum, Y., Krooss, B.M., Littke, R., 2014. Experimental study of fluid transport processes in the matrix system of the European organic-rich shales: II Posidonia shale. Int. J. Coal Geol. 123, 20–33.
Herber, R., de Jager, J., 2010. Oil and gas in the Netherlands – is there a future?, Netherlands Journal of Geoscience, 89–2, 91–107.
Hesselbo, S.P., Gröcke, D.R., Jenkyns, H.C., Bjerrum, C.J., Farrimond, P., Morgans Bell, H.S., Green, O.R., 2000. Massive dissociation of gas hydrate during a Jurassic oceanic anoxic event. Nature 406, 392–395.
Hilger, J., 2003. Combined Utilization of Oil Shale Energy and Oil Shale Minerals within the Production of Cement and Other Hydraulic Binders, Oil Shale. Vol. 20, 3. pp. 347–355.
Hol, S., Spiers, C.J., 2012. Competition between adsorption-induced swelling and elastic comperssion of coal at CO2 pressures up to 100MPa. Journal of Mechanics and Physics of Solids 60, 1862–1882.
Houben, M.E., Desbois, G., Urai, J.L., 2013. Pore morphology and distribution in the Shaly facies of Opalinus clay (Mont Terri, Switzerland): insights from representative 2D BIB-SEM investigations on mm to nm scale. Appl. Clay Sci. 71, 82–97.
Houben, M.E., Desbois, G., Urai, J.L., 2014. A comparative study of representative 2D microstructures in shale and Sandy facies of Opalinus clay (Mont Terri, Switzerland) inferred from BIB-SEM and MIP methods. Mar. Pet. Geol. 49, 143–161.
Houben, M.E., Barnhoorn, A., Lie-A-Fat, J., Ravestein, T., Peach, C.J., Drury, M.R., 2016a. Microstructural characteristics of the Whitby mudstone formation (UK). Mar. Pet. Geol. https://doi.org/10.1016/j.mapetgeo.2015.11.011.
Houben, M.E., Barnhoorn, A., Wasch, L., Trabucho-Alexandre, J., Peach, C., Drury, M.R., 2016b. Microstructures of early Jurassic (Toarcian) shales of northern Europe. Int. J. Coal Geol. 165, 76–89.
Kanitpanyacharoen, W., Kets, F.B., Wenk, H.-R., Wirth, R., 2012. Mineral preferred orientation and microsturcture in the Posidonia shale in relation to different degrees of thermal maturity. Clay Clay Miner. 60, 315–329.
Klaver, J., Desbois, G., Urai, J.L., Littke, R., 2012. BIB-SEM study of the pore space morphology in early mature Posidonia shale from the Hils area, Germany. Int. J. Coal Geol. 103, 12–25.
Klaver, J., Desbois, G., Littke, R., Urai, J.L., 2016. BIB-SEM pore characterization of mature and post mature Posidonia shale samples from the Hils area, Germany. Int. J. Coal Geol. 158, 78–89.
Littke, R., Baker, D.R., Leythaeuser, D., Rullkötter, J., 1991. Keys to the depositional history of the Posidonia shale (Toarcian) in the Hils syncline, northern Germany, from: Tyson, R.V., Pearson, T.H. (eds), modern and ancient continental shelf anoxia. Geol. Soc. Spec. Publ. 58, 331.
Liu, J., Peach, C.J., Spiers, C.J., 2016a. Anisotropic swelling behavior of coal matrix cubes exposed to water vapour: effects of relative humidity and sample size. Int. J. Coal Geol. 167, 119–135.
Liu, Y., King, H.E., van Huis, M.A., Drury, M.R., Plümper, O., 2016b. Nano-tomography of porous geological materials using focused ion beam – scanning Electron microscopy. Fortschr. Mineral. 6, 104. https://doi.org/10.3390/min6040104.
Mathia, E.J., Bowen, L., Thomas, K.M., Aplin, A.C., 2016. Evolution of porosity and pore types in organic-rich, calcareous, lower Toarcian Posidonia shale. Mar. Pet. Geol. 75, 117–139.
Minardi, A., Crisci, E., Ferrari, A., Laloui, L., 2016. Anisotropic Volumetric Response of Shales upon Suction Changes. EAGE.
Powell, J.H., 2010. Jurassic sedimentation in the Cleveland Basin: a review. Proc. Yorks. Geol. Soc. 58 (1), 21–72.
Rexer, T.F., Mathia, E.J., Aplin, A.C., Thomas, K.M., 2014. High-pressure methane adsorption and characterization of pores in Posidonia shales and isolated kerogens. Energy Fuel 28, 2886–2901.
Seemann, T., Bertier, P., Krooss, B.M., Stanjek, H., 2017. Water vapour sorption on mudrocks, in: Rutter, E.H., Mechlenburgh, J., Taylor, K.G., eds. Geomechanical and petrophysical properties of mudrocks, Geological Society of London, Special Publications, 454, pp. 33.
Soe, A.K.K., Osada, M., Takahashi, M., Sasaki, T., 2009. Characterisation of drying-induced deformation behavior of Opalinus clay and tuff in no-stress regime. Environ. Geol. 58, 1215–1225.
Stokes, D.J., 2006. Progress in the specimens using study of biological ESEM. In Focus – the Proceedings of the Royal Microscopical Society 2, 10.
Ter Heege, J., Zijp, M., Nelskamp, S., Douma, L., Verreussel, R., Ten Veen, J., de Bruin, G., Peters, R., 2015. Sweet spot identification in underexplored shales using multi-disciplinary reservoir characterization and key performance indicators: example of the Posidonia shale formation in the Netherlands. Journal of Natural Gas Science and Engineering 27, 558–577.
Trabucho-Alexandre, J., Dirkx, R., Veld, H., Klaver, G., de Boer, P.L., 2012. Toarcian black shales in the dutch central graben: record of energetic, variable depositional conditions during an oceanic anoxic event. J. Sediment. Res. 82, 104–120.
Zhang, C.L., Wieczorek, K., Xie, M.L., 2010. Swelling experiments on mudstones. J. Rock Mech. Geotech. Eng. 2, 44–51.
Zhubayev, A., Houben, M.E., Smeulders, D.M.J., Barnhoorn, A., 2015. Ultrasonic velocity and attenuation anisotropy of shales, Whitby. United Kingdom, Geophysics 81, D45–D56.